NE-CAT COMMUNICATIONS

A Biannual Newsletter of the Northeastern Collaborative Access Team Summer 2010

A Message from the Director
Steven Ealick

It has been a hot summer and an equally hot time at NE-CAT. NE-CAT has had a very exciting and productive half a year.

In May 2009, NE-CAT applied for a high end equipment grant from NCRR to fund the purchase of a Pixel Array Detector (PAD). As a class, PADs are generally acknowledged as the near-term successor to CCD's at 3rd generation synchrotron crystallography beamlines. The PILATUS-6M, from Dectris Ltd., is the first commercially available PAD suitable for synchrotron-based macromolecular crystallographic data collection. I am happy to report that our application has been approved and we are moving forward with the purchase of the PILATUS-6M detector.

PILATUS-6M offers many advantages over the current CCD detectors. The main advantages of a pixel array detector include: no leakage current or readout noise, superior signal-to-noise ratio, a fast read-out time of 3.5 ms, a sustained 12.5 Hz frame rate, a much higher effective dynamic range, and the possibility to suppress fluorescence by a energy threshold that is set individually for each pixel. The short readout and fast framing time also allow collection of diffraction data in continuous mode without opening and closing the shutter for each frame. Additional information on the advantages of pixel array detectors and the PILATUS-6M, in particular, is available later in this newsletter.

In the last newsletter, I mentioned that we had received an administrative supplement from NCRR. A 128 core computing cluster and a new data storage array purchased with this money have arrived. We have also enhanced our sample automounter program through the purchase of additional cryopucks and tools. These tools are central to our puck loaning program which is described in greater detail later in this newsletter. We have also filled the positions funded by the administrative supplement. I would like to welcome Surajit Banerjee and Amit Belani to NE-CAT. Surajit will be assisting in our sample automounter program and user program. Amit will be assisting our Core 3 research in addition to managing our computers, data storage and network. You can learn more about them later in the newsletter.

If you have not taken the opportunity to use NE-CAT's beamlines to date, I encourage you to do so in the future. For further information on our beamline capabilities and how to request time, please visit our website at http://necat.chem.cornell.edu.

Beamline Developments

1. Beam Position Monitors Move

During the May shutdown, the beam position monitors (BPMs) on 24-ID-E were moved upstream from their attached position on the MD2 lift mechanism. This also places the beam position monitors upstream of the attenuators. The old location of the BPMs maximized beam stability but required a fixed attenuation setting for beam-steering. Due to timing issues, this resulted in doubly-exposed images on occasion. The upstream move of the BPMs eliminates the need for a fixed attenuation setting during beam steering.

2. Computer Processor Upgrade

On both beamlines, the old processors for the master and auxiliary beamline control computers were replaced with Intel I7s. Also the data collection computers were upgraded to Intel I7s with powerful graphics cards to drive the newly installed high resolution 30-inch LCD monitors. In additional computer news, the hardware for the new 128 core computing cluster has arrived from TeamHPC and been commissioned at our facility. Also, a 42 terabyte SATABeast data storage array has been received from NexSan and configured for our use. This brings our total data storage capacity to 72 terabytes.

3. Detector Refurbishment

The three Q315 detectors and their associated frame grabbers are being systematically sent back to ADSC for refurbishment and software upgrades. The Q315 detector from 8-BM was sent to ADSC during the January shutdown. It was followed by the Q315 detector on 24-ID-C during the May shutdown. Both of the detectors returned within one month. The Q315 detector on 24-ID-E (Fig. 1) was removed on August 26 and shipped to ADSC for refurbishment during the September shutdown.

Figure 1. Q315 Detector being removed from the A-Frame in the 24-ID-E hutch in preparation for refurbishment.

As part of the refurbishment, the former 8-BM detector and frame grabbers received software upgrades. The phosphors on both detectors were replaced and the detectors were re-calibrated. With the refurbishment and upgrades, the former 8-BM detector can now serve as a drop-in spare for either ID beamline while 24-BM is being constructed. After re-installment of the refurbished detector on 24-ID-C, quality assurance trials were performed. These trials show a reduction in background noise and overall improvement in data quality.

4. RAPD

With difficult crystallographic problems, such as microcrystals, an optimal data collection strategy is necessary for complete data collection. During 2009, the EDNA online data analysis (ODA) environment was tested at NE-CAT to perform data analysis as part of Core 3 research. Unfortunately, EDNA did not meet our goals. Hence, we chose to create our own ODA environment which we have dubbed RAPD (**R**apid **A**utomated **P**rocessing of **D**ata).

RAPD is designed as a series of independent modules (Fig. 2). The modules function together to monitor data collection, store information regarding collected raw data, process initial images and runs, store information regarding processing results and to present results to users in an interactive web user interface (UI) designed for remote login. The major components of RAPD include:

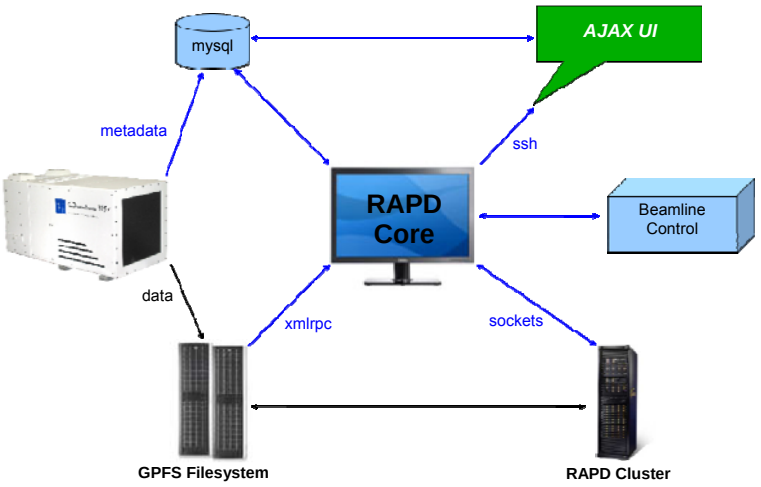

Figure 2. RAPD dataflow architecture.

- RAPD Core – This process coordinates data collection monitoring, dispatches jobs to the cluster, logs results into the database, communicates with the beamline and monitors the database for remotely-initiated processes. As its name denotes, this is the central hub of RAPD.
- RAPD Cluster – This module performs the data analysis at the direction of the RAPD Core. The RAPD Cluster has a number of specialized agents for different data analysis functions. Each agent wraps multiple data analysis programs for autoindexing, strategy, integration, etc.
- MySQL Database – This stores metadata on raw images and results. The database is used both to construct the UI and to coordinate actions initiated from the UI.
- AJAX UI – The UI is designed so that it can be viewed via a web browser from anywhere. The UI provides data processing results as text, tables and images. Commands and settings can be sent to the RAPD Core via the UI.

RAPD has become very popular among our users for providing data collection strategies, even when using the mini-Kappa goniometer head. Many more enhance-

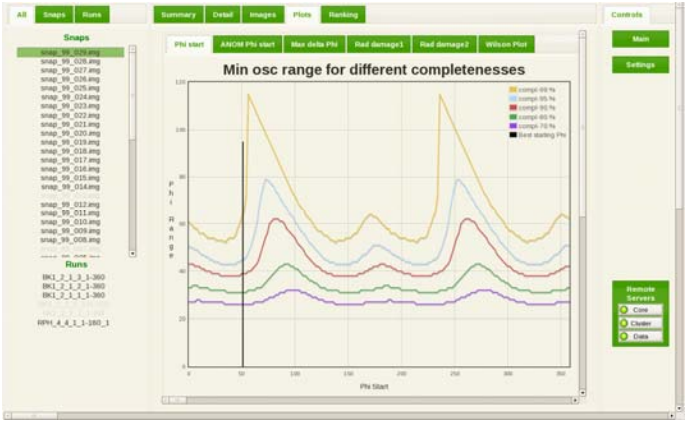

Figure 3. RAPD User Interface (UI).

ments to the ODA are in the pipeline, so be sure to try out RAPD during your next visit to NE-CAT.

5. Puck Loan Program

Our second generation sample automounter have been operating flawlessly on NE-CAT beamlines for over a year. To increase use of the sample automounters, NE-CAT has initiated a new puck loan program. Previously, if a user did not own automounter-compatible cryopucks and tools, it was possible to load samples into NE-CAT cryopucks on-site using the NE puck loading tool. This tool is still available, but as part of the puck loan program, a user can borrow a set of cryopucks and associated tools for loading pucks at their home institution. NE-CAT has purchased over a hundred new ALS-style pucks, related shipping canes and shipping hooks. Pucks and their associated equipment will be shipped out in their own packing case. Users interested in participating in the loan program should see our web page.

Figure 4. Shipping kit for loaner pucks. Kit includes cryopucks, shipping cane, shipping cane hook, bent cryopuck tongs, puck separator, puck wand and stand for stabilizing pucks.

PILATUS-6M

The current ADSC Q315 large area detectors in use on both NE-CAT beamlines are indirect detection systems, where an X-ray phosphor is optically coupled to a 2D CCD detector. On the other hand, a PAD is a direct detection system. PILATUS detectors are comprised of two-dimensional hybrid PADs, which operate in single-photon counting mode. Each hybrid pixel (or Read Out Unit, ROU) comprises a preamplifier, a comparator and a counter. The preamplifier enforces the charge generated in the sensor by the incoming X-ray; the comparator produces a digital signal if the incoming charge exceeds a predefined threshold and thus, together with the counter, one obtains a complete digital storage and read-out of the number of detected X-rays per pixel without any read-out noise or dark current! The PILATUS-6M consists of a roughly symmetric tiling of 60 PAD modules, each measuring 487x195 pixels.

As our microcrystallography program has developed, we are running up against performance limitations of the Q315 in principally three areas: 1) read out and dark current noise, 2) low dynamic range and linearity, and 3) slow read out speed. The following table compares salient operational characteristics between the ADSC Q315 and the PILATUS-6M detectors.

Property / Characteristic	ADSC Q315	PILATUS-6M
Detector Type	Integrating	Photon Counter
Active Area (mm x mm)	315 x 315	431 x 448
Edge Pixel Count	6000 x 6000	2527 x 2463
Pixel Size (microns)	50 x 50 (90 x 90 w. PS)	172 x 172
Pixel Counting Depth	65536	1048575
Detector Module Tiling	3 x 3	12 x 5
Tiling Gap (mm)	0.4 x 0.4	1.77 x 2.72
Read Out Time (msec)	350 (2x2 binned) 1250 (full res)	3.5
Image Size (Mbytes)	~18.6 (2x2 binned) ~74 (unbinned)	25
Max Counting Rate /Pixel/sec	Unlimited	1.5 MHz
Signal / Noise Limiting Factor	Dark Current, Read Noise	Fluorescence Background
Detective Quantum Efficiency	~80% 12 KeV	~80% 12 KeV
Approximate Cost (thousands $)	850	1500

Read Out Noise, Dynamic Range and Differential Non-linearity

The PILATUS-6M will improve our ability to measure weak high order reflection data or data from small or

poorly diffracting crystals by eliminating read out noise and dark current.

Small crystals generally produce high resolution spot intensities only marginally above local background. The NE-CAT beamline optics, used in conjunction with the Maatel MD2 microdiffractometer beam shaping system, produces very low background scatter and fluorescence. Noise in diffraction data frames, at resolutions greater than the water ring (< 3.5 Å), derives from ice matrix scatter, dark current and read out noise of the ADSC Q315 detector. In the absence of ice, the dominant source of noise comes from the CCD dark current.

PAD detectors are sensitive to incoming X-ray photons only when the PAD read out units are gated to count photons. As a discrete array of photon counters, the PILATUS ROUs manifest essentially zero read out noise and zero dark noise. CCD detectors accumulate photon-induced charge at all times (even during readout) and manifest significant time-dependent dark count noise due to leakage currents within the CCD device.

Due to the fact that the Q315 readout provides only 16 bits of dynamic range (counting depth of 65536), low order diffraction spots tend towards saturation under conditions optimized for accuracy in high order diffraction measurements. The Q315 also shows increased differential nonlinearity. Thus, well before low order spots have achieved saturation one experiences systematic undercounting due to the nonlinearity of the Q315 readout system.

The event counters of each PILATUS ROU have 20 bits of resolution (counting depth of 1048575), 16-times that of the Q315. This is a dramatic increase in dynamic range.

Read Out Speed and Shutterless Operation

The 3.5 ms readout speed of the PILATUS-6M is 100 times faster than the Q315. The gate-ability and high read out speed of PADs enable data collection strategies that are not feasible with CCD-based systems, notably shutterless data collection and extreme fine phi-slicing. Shutterless data collection is only possible with an electronically gate-able detector. With this method, the sample goniometer is accelerated to constant angular velocity, and the PAD array is gated to count and readout at a constant period. Exposure time is then just the interval between successive gatings and readouts. This method of data collection completely eliminates the time-cost and errors associated with goniometer-shutter synchronization. Since CCDs are not gate-able, they are not ideal for shutterless data collection.

Resolution and Image Corrections

The PILATUS-6M has a large pixel size (172 x 172 µ) compared to the ADSC Q315 (50 x 50 µ). However, since there is negligible charge transfer between contiguous PAD pixels, PAD detectors manifest zero point spread. On the other hand, the continuous phosphor sheet used by CCD detectors to convert impinging X-ray photons to visible light induces a large point spread or blurring of the effective pixel size. The point spread function of CCDs varies as a function of detection position, being large at the edges or corners of the fiber optic taper. This is the so-called "corner-effect" that is responsible for higher errors at certain resolution shells, specifically for samples with rather low mosaicity. The Q315 point spread function varies between 90 and 120 microns.

In contrast PAD detectors have zero point spread function. Therefore, the large pixel size of the PILATUS, compared to the Q315, is compensated by the larger coverage and zero point spread pixel of the PILATUS.

Summary

Overall, the installation of a PILATUS-6M at 24-ID-C is expected to result in a 3- to 5-fold improvement in data collection rates due to its low read out time and improve data quality because of elimination of synchronization errors in the framing cycle of shutter, goniometer and detector systems. We expect data quality improvement due to lack of readout noise and absence of dark current. These improvements, coupled with efficient sample loading automation will leverage the value of the beamline by reducing time required for sample survey and increasing the number of high quality data sets acquired during each user visit. Additionally, the high speed of the PILATUS will make feasible data collection strategies and operational methods not practical with CCD detectors.

Research Highlights

The Structural Basis of Ion Channel Gating

Eduard Perozo, Department of Biochemistry and Molecular Biology, The University of Chicago, Chicago, IL

Potassium channels are membrane proteins that catalyze the transfer of K^+ ions down an electrochemical gradient with high efficiency and selectivity. Their function has been associated with such basic cellular functions as the regulation of electrical activity, signal transduction and osmotic balance. K^+ channels are members of the voltage-dependent channel superfamily, which include explicitly voltage-activated channels (Na^+, Ca^{++}, and a large number of K^+ channels), as well as voltage-independent channels (i.e., the inward rectifiers and the

cyclic nucleotide activated channels).

The minimal K^+ channel gating mechanism requires two gates, an activation gate that can be open or closed (i.e., the inner-bundle helix), and an inactivation gate that can exist in two conformations, conductive or non-conductive (Inactivated) (Ben-Abu et al., 2009; Cordero-Morales et al., 2006; Panyi and Deutsch, 2006). For the prokaryotic K^+ channel KcsA, the structure of the Closed-Conductive state has been known for some time at very high resolution (Doyle et al., 1998; Zhou et al., 2001). Over the past four years, we have made extensive use of the NE-CAT beamlines and benefited from the insight and expertise of the support staff. Thanks to the excellent stability, intensity and homogeneity of the beamline, we were able to determine several structures of a KcsA construct trapped with an open inner gate (Cuello et al., 2010b), including the Open-Inactivated state (Cuello et al., 2010a). These structures provide a thorough description of the inactivated filter and help define the structure of all discreet functional states of the K^+ channel gating cycle.

Development of a constitutively open channel mutant amenable to crystallographic analyses (OM-KcsA) made possible the determination of a variety of crystal structures of KcsA in its key functional states. By establishing the molecular elements responsible for proton sensitivity in KcsA, we engineered a constitutively open-channel in which the inner helical bundle is fully open at neutral and basic pH (Cuello et al., 2010b). After engineering the crystal lattice by gradually reducing the size of the N-terminal helix, we were able to obtain a fully open KcsA structure at a resolution of 3.2 Å (Cuello et al., 2010a) (Fig. 4).

Analysis of this structure revealed significant conformational changes at the selectivity filter, including a compression of the permeation path at G77, a putative flipping of carbonyl groups at V76 (not well resolved at 3.2 Å) and a reduction in ion occupancy at potassium binding sites S2 and S3 (Fig. 5). This structure is reminiscent to the low K^+ structure observed by Zhou et al (Zhou et al., 2001), yet takes place in the presence of 200-300 mM K^+, supporting the idea that the selectivity filter can enter a common non-conductive conformation chemically or allosterically.

Remarkably, in the process of screening crystals for the fully Open-Inactivated structure, we also identified intermediate states with different degrees of opening at the bundle crossing and different extents of inactivation corresponding to multiple partially closed and open-inactivated states. We solved a total of 15 non-redundant KcsA structures "trapped" in different stages along the transition pathway, including at least four classes of gating intermediates (Cuello et al., 2010a).

The KcsA inner helical bundle can be stabilized with several degrees of gate opening, ranging from about 11.5 Å in the closed state (Ca-Ca distances in 1K4C at position T112) to 32 Å in the fully open state, plus defined stable structures at 14, 15, 17 and 23 Å. Analysis of these structures revealed that the conformational changes at the selectivity filter strongly correlated with the degree of opening at the inner helix bundle and are accompanied by a progressive loss of ion occupancy at binding sites S2 and S3 (Fig. 5). Based on these findings we proposed an explicit mechanism for C-type in-

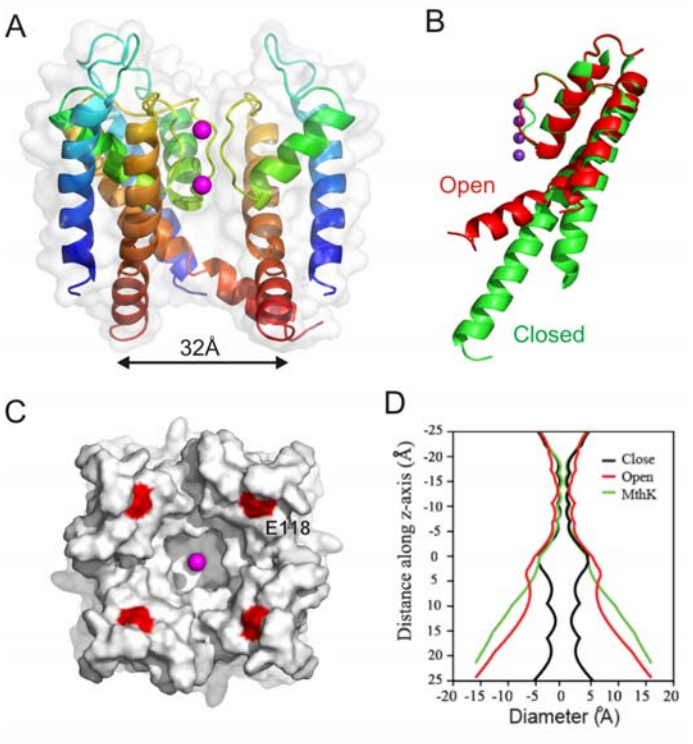

Figure 4. Structure of Open-Inactivated OM-KcsA. A. Oligomer showing its 32 Å opening**. B.** Comparson of open and closed monomers. **C.** Intracellular view highlighting location of E118. **D.** Hole profile comparing Open KcsA, Closed KcsA and MthK.

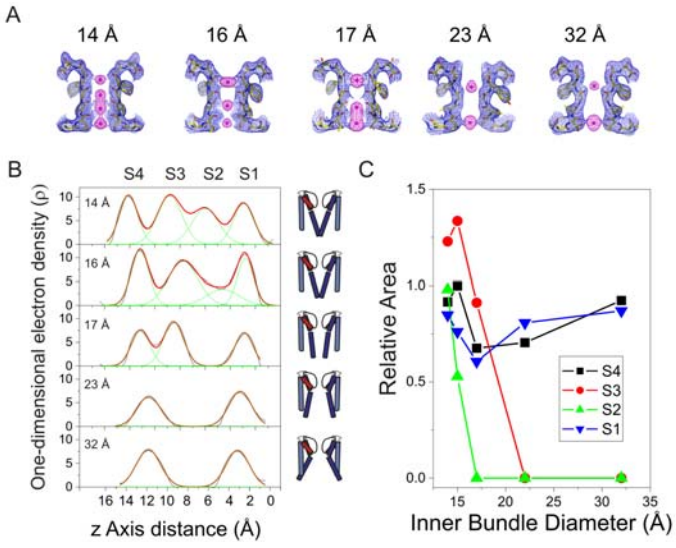

Figure 5. Dependence of filter ion occupancy with the degree of opening in the inner bundle gate. **A.** Electron densities for five structural classes of the selectivity filter. **B.** One dimensional electron density of ion occupancy in the four binding sites. **C.** Correlation between estimated occupancy (peak area) and inner gate opening (in Å).

activation based on the notion that the K^+ selectivity filter is unable to conduct ions when two sequential ion binding sites (S2 and S3) are compromised by rearrangements in the backbone conformation at or near Gly77. These structures, and the methods developed to obtain them have opened a wealth of experimental options by offering an explicit path towards the structural basis of a wide range of functionally important mutants and/or ion-channel interactions.

References

Ben-Abu, Y., Zhou, Y., Zilberberg, N., and Yifrach, O. (2009). Inverse coupling in leak and voltage-activated K^+ channel gates underlies distinct roles in electrical signaling. Nat Struct Mol Biol *16*, 71-79.

Cordero-Morales, J.F., Cuello, L.G., Zhao, Y., Jogini, V., Cortes, D.M., Roux, B., and Perozo, E. (2006). Molecular determinants of gating at the potassium-channel selectivity filter. Nat Struct Mol Biol *13*, 311-318.

Cuello, L.G., Jogini, V., Cortes, D.M., and Perozo, E. (2010a). Structural mechanism of C-type inactivation in K^+ channels. Nature *466*, 203-208.

Cuello, L.G., Jogini, V., Cortes, D.M., Sompornpisut, A., Purdy, M.D., Wiener, M.C., and Perozo, E. (2010b). Design and characterization of a constitutively open KcsA. FEBS Lett *584*, 1133-1138.

Doyle, D.A., Cabral, J.M., Pfuetzner, R.A., Kuo, A., Gulbis, J.M., Cohen, S.L., Chait, B.T., and MacKinnon, R. (1998). The structure of the potassium channel: molecular basis of K^+ conduction and selectivity [see comments]. Science *280*, 69-77.

Panyi, G., and Deutsch, C. (2006). Cross talk between activation and slow inactivation gates of Shaker potassium channels. J Gen Physiol *128*, 547-559.

Zhou, M., Morais-Cabral, J., Mann, S., and MacKinnon, R. (2001). Potassium channel receptor site for the inactivation gate and quaternary amine inhibitors. Nature *411*, 657-661.

Diphthamide biosynthesis requires an organic radical generated by an Fe-S enzyme

Steven E. Ealick, Department of Chemistry and Chemical Biology, Cornell University, Ithaca, NY

Our entry into the radical *S*-adenosylmethionine (SAM) field came pretty much by accident. In fact, the enzyme described in this report was not predicted to be a radical SAM enzyme prior to our structural studies. Radical SAM enzymes generally use a reduced [4Fe-4S] cluster to homolytically cleave the C-S bond of SAM resulting in an adenosyl radical and methionine. The adenosyl radical is then used to initiate downstream reactions typically by abstracting a very basic proton. The radical SAM superfamily is thought to be very large (perhaps thousands of enzymes) but only a few dozen have been biochemically characterized and only a handful of structures are available. Members of the radical SAM superfamily have a b-barrel or modified b-barrel structure. The [4Fe-4S] cluster is found in the loop following b1 and buried in the b-barrel cavity. Three cysteine residues, usually found in a CxxxCxxC motif, bind the [4Fe-4S] cluster.

Contributors to structural work on Dph2 (left to right): Yang Zhang, Andrew T. Torelli, Steven E. Ealick

Dph2 is a SAM-dependent archael enzyme involved in the biosynthesis of diphthamide, which is a postranslationally modified histidine residue. The modification occurs only in elongation factor 2 (EF2) and requires (i) transfer of a 3-amino-3-carboxypropyl group to C2 of histidine, (ii) trimethylation of the amino group, and (iii) amidation of the carboxy group. The modification is important for the translocation step of ribosomal protein synthesis and is conserved in all eukaryotes and archaea. Dph2 catalyzes the first step of the modification. The modification is called diphthamide because it is the target of diphtheria toxin, which inactivates EF2 by catalyzing ADP-ribosylation of diphthamide resulting in cell death.

Initial attempts to reconstitute Dph2 activity were unsuccessful; however, we were able to crystallize the enzyme. The structure showed Dph2 to be a homodimer. Each monomer is composed of three structurally homologous domains suggesting a gene triplication and fusion event. Each domain contributes several conserved residues that cluster in the center of each monomer. The most striking feature was the presence of three cysteine residues, one from each domain, in the cluster of conserved residues. While the cysteine residues are in different domains and separated by roughly 100 amino acid residues, their geometrical arrangement was reminiscent of the cysteine residues that bind the [4Fe-4S] cluster in radical SAM enzymes, suggesting that Dph2 might also contain a [4Fe-4S] cluster.

We then added sources of iron and sulfur during protein expression and carried out the purification in a glove box. Using radiolabeled SAM we showed for the first time that Dph2 catalyzes the first step of diphthamide biosynthesis. In addition, we crystallized the anaerobically purified Dph2 and the structure showed the [4Fe-

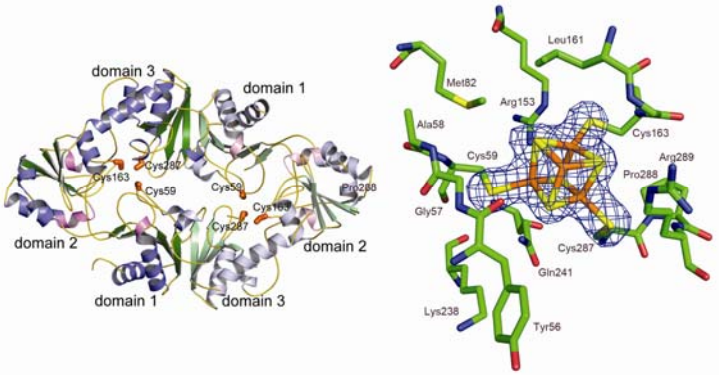

On the left is the structure of *Pyrococcus horikoshii* Dph2 (PDB ID 3LZC) and on the right the difference density for the [4Fe-4S] cluster in reconstituted Dph2 (PDB ID 3LZD).

4S] cluster. What remained was to propose a reaction mechanism. Nucleophilic attack was a possibility but the histidine C2 atom is a poor nucleophile. Instead we thought that maybe Dph2 utilizes an aminocarboxypropyl radical. This organic radical has never been proposed in an enzyme mechanism. The proof for this hypothesis came from observing the product in the presence of SAM and reducing agent but in the absence of EF2. The product was 2-aminobutyric acid, which only could have been generated by quenching an aminocarboxypropyl radical. In this case, the crystal structure led to the identification of both a novel radical SAM enzyme and a novel organic radical. The details of the studies described here were recently published (*Nature* **465**: 891-896, 2010).

NE-CAT New Hires

As stated in the previous newsletter, NE-CAT received an administrative supplement in October 2009 and was in the process of hiring two new staff members, a postdoctoral associate and a computer programmer. This spring, both positions were filled and the new staff members joined NE-CAT.

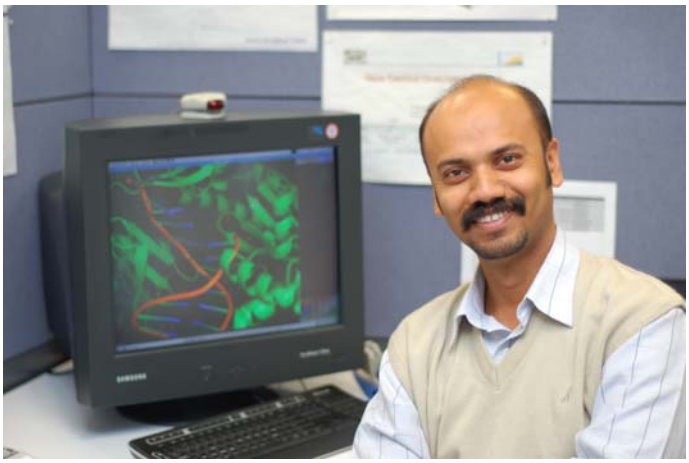

Postdoctoral associate, Surajit Banerjee, joined NE-CAT in May 2010. He obtained his PhD in X-ray crystallography from the Physics Department of Jadavpur University, Kolkata, India. Afterwards, he worked at Dr. Reddy's Lab, a pharmaceutical company in Hyderabad, India, investigating polymorphism in drug candidates. Surajit joined the Nephrology-Medicine Department of Vanderbilt University, TN and worked on the structure of the Non-Collagenous (NC1) domain of type IV collagen. Afterwards, he moved to the lab of Dr. Michael P. Stone, in the Department of Chemistry at Vanderbilt University, where he used NMR and X-ray crystallography to determine the structure of duplex DNA and polymerase-DNA complexes with carcinogen-modified oligonucleotides. At NE-CAT Surajit will be responsible for user support and enhancing the sample automounter program.

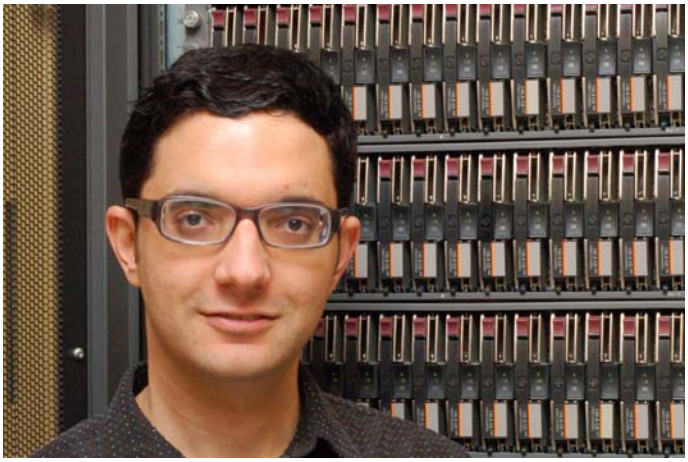

Amit Belani joined NE-CAT as Computer Operations Manager in June 2010. He has a Master of Engineering degree in Computer Science from Cornell University, and a B.S. degree in Computer Science from Mercy College, NY. In addition he has professional experience in software development with C and Python, and in server administration. His interests lie primarily in software development for high-performance scientific computing, and also in machine learning and data visualization. Amit will be assisting Core 3 research (software for challenging problems) in addition to managing our computers, data storage and network infrastructure.

Staff Activities

Talks

Kanagalaghatta Rajashankar & Igor Kourinov, "Collecting Two-Wavelength MAD Data Without Changing Energy!" CLS 13th Annual Users' Meeting in Saskatoon, Saskatchewan, Canada, June 17-18, 2010

Kanagalaghatta Rajashankar, "MAD data collection strategies for crystals with weak anomalous signal and weak diffraction," Macromolecular Crystallography Stream CLS Summer School in Saskatoon, Saskatchewan, Canada, June 13th, 2010

Kanagalaghatta Rajashankar & Igor Kourinov, "Collecting Two-Wavelength MAD Data Without Changing Energy!" 2010 Annual Meeting of the American Crystallographic Association, Chicago, Illinois, July 24-29, 2010

Narayanasami Sukumar, "Role of Protein Dynamics in Electron Transfer – A Joint X-ray and Neutron Study on a Copper Protein," Material Research Society (MRS) Meeting – ACNS2010 (American Conference on Neutron Scattering) in Ottawa, Canada, June 26-30, 2010

Posters

Narayanasami Sukumar, Scott Mathews, Paul Langan, Victor Davidson, “A Joint X-ray and Neutron Diffraction Study on a Copper Protein Reveal the Role of Protein Dynamics in Electron Transfer,” 2010 Annual Meeting of the American Crystallographic Association, Chicago, Illinois, July 24-29, 2010

Jon Schuermann, David Neau, Kanagalaghatta Rajashankar, Frank Murphy, “Rapid Automated Processing of Data (RAPD) Software Package,” 2010 Annual Meeting of the American Crystallographic Association, Chicago, Illinois, July 24-29, 2010

Kay Perry, Malcolm Capel, Surajit Banerjee, Amit Belani, Igor Kourinov, Ed Lynch, Frank Murphy, David Neau, Kanagalaghatta Rajashankar, Cynthia Salbego, Jonathan Schuermann, Narayanasami Sukumar, James Withrow & Steven E. Ealick, “Collaborative Access Team (NE-CAT) Beamlines at the Advanced Photon Source,” 2010 Annual Meeting of the American Crystallographic Association, Chicago, Illinois, July 24-29, 2010

Surajit Banerjee, Plamen P. Christov, Albena Kozekova, Carmelo J. Rizzo, Michael P. Stone, “Structural Investigation of trans-4-hydroxynonenal-derived 1,N^2-deoxyguanosine Adduct in protein-DNA complex,” 2010 Annual Meeting of the American Crystallographic Association, Chicago, Illinois, July 24-29, 2010

Jon Schuermann, David Neau, Kanagalaghatta Rajashankar, Frank Murphy, “Rapid Automated Processing of Data (RAPD) Software Package,” Gordon Research Conference on Diffraction Methods in Structural Biology in Lewiston, Maine, July 18-23, 2010.

Narayanasami Sukumar, “Structural and Postcrystallization Analysis on Human Intrinsic Factor-Cobalamin Complex,” Keystone Symposia on Structural Biology in Silverthrone, Colorado, January 8-13 2010.

Publications

Khare, B., Samal, A., Vengadesan, K., Rajashankar, K. R., Ma, X., Huang, I. H., Ton-That, H., and Narayana, S. V. (2010) Preliminary crystallographic study of the Streptococcus agalactiae sortases, sortase A and sortase C1, *Acta Crystallogr. F 66*, 1096-1100.

Himanen, J. P., Yermekbayeva, L., Janes, P. W., Walker, J. R., Xu, K., Atapattu, L., Rajashankar, K. R., Mensinga, A., Lackmann, M., Nikolov, D. B., and Dhe-Paganon, S. (2010) Architecture of Eph receptor clusters, *Proc. Natl. Acad. Sci. U. S. A. 107*, 10860-10865.

Kovalevsky, A. Y., Fisher, S. Z., Seaver, S., Mustyakimov, M., Sukumar, N., Langan, P., Mueser, T. C., and Hanson, B. L. (2010) Preliminary neutron and X-ray crystallographic studies of equine cyanomethemoglobin, *Acta Crystallogr. F* 66, 474-477.

Sukumar, N., Mathews, F. S., Langan, P., and Davidson, V. L. (2010) A joint X-ray and neutron study on amicyanin reveals the role of protein dynamics in electron transfer, *Proc. Natl. Acad. Sci. U. S. A. 107*, 6817-6822.

Malakhova, M., D'Angelo, I., Kim, H. G., Kurinov, I., Bode, A. M., and Dong, Z. (2010) The crystal structure of the active form of the C-terminal kinase domain of mitogen-and stress-activated protein kinase 1. *J. Mol. Biol. 399,* 41-52.

Paul, D., O'Leary, S. E., Rajashankar, K., Bu, W., Toms, A., Settembre, E. C., Sanders, J. M., Begley, T. P., and Ealick, S. E. (2010) Glycal Formation in Crystals of Uridine Phosphorylase. *Biochemistry 49, 3499-3509.*

Larson, M. R., Rajashankar, K. R., Patel, M. H., Robinette, R. A., Crowley, P. J., Michalek, S., Brady, L. J., and Deivanayagam, C. (2010) Elongated fibrillar structure of a streptococcal adhesin assembled by the high-affinity association of α- and PPII-helices, *Proc. Natl. Acad. Sci. U. S. A.* 107, 5983-5988.

Gu, M., Rajashankar, K. R., and Lima, C. D. (2010) Structure of the *Saccharomyces cerevisiae* Cet1-Ceg1 mRNA Capping Apparatus, *Structure* 18, 216-227.

Schuermann, J. P., Tan, A., Tanner, J. J., and Henzl, M. T. (2010) Structure of Avian Thymic Hormone, a High-affinity Avian β-parvalbumin, in the Ca^{2+}-free and Ca^{2+}-bound States, *J. Mol. Biol. 397*, 991-1002.

Srivastava, D., Schuermann, J. P., White, T. A., Krishnan, N., Sanyal, N., Hura, G. L., Tan, A., Henzl, M. T., Becker, D. F., and Tanner, J. J. (2010) Crystal structure of the bifunctional proline utilization A flavoenzyme from *Bradyrhizobium japonicum*, *Proc. Natl. Acad. Sci. U. S. A. 107*, 2878-2883.

Perry, K., Hwang, Y., Bushman, F. D., and Van Duyne, G. D. (2010) Insights from the Structure of a Smallpox Virus Topoisomerase-DNA Transition State Mimic, *Structure 18*, 127-137.

Acknowledgements

NE-CAT is supported by Grant (RR-15301) from the NIH National Center for Research Resources and contributions from the following NE-CAT institutional members: Columbia University, Cornell University, Harvard University, Massachusetts Institute of Technology, Memorial Sloan-Kettering Cancer Center, Rockefeller University, and Yale University